Supplementary material for "Optimized selectivity in CO_2 electrochemical reduction using amorphous CuNi catalysts: insights from density functional theory and machine learning simulations"

Accuracy of the machine learning forcefield

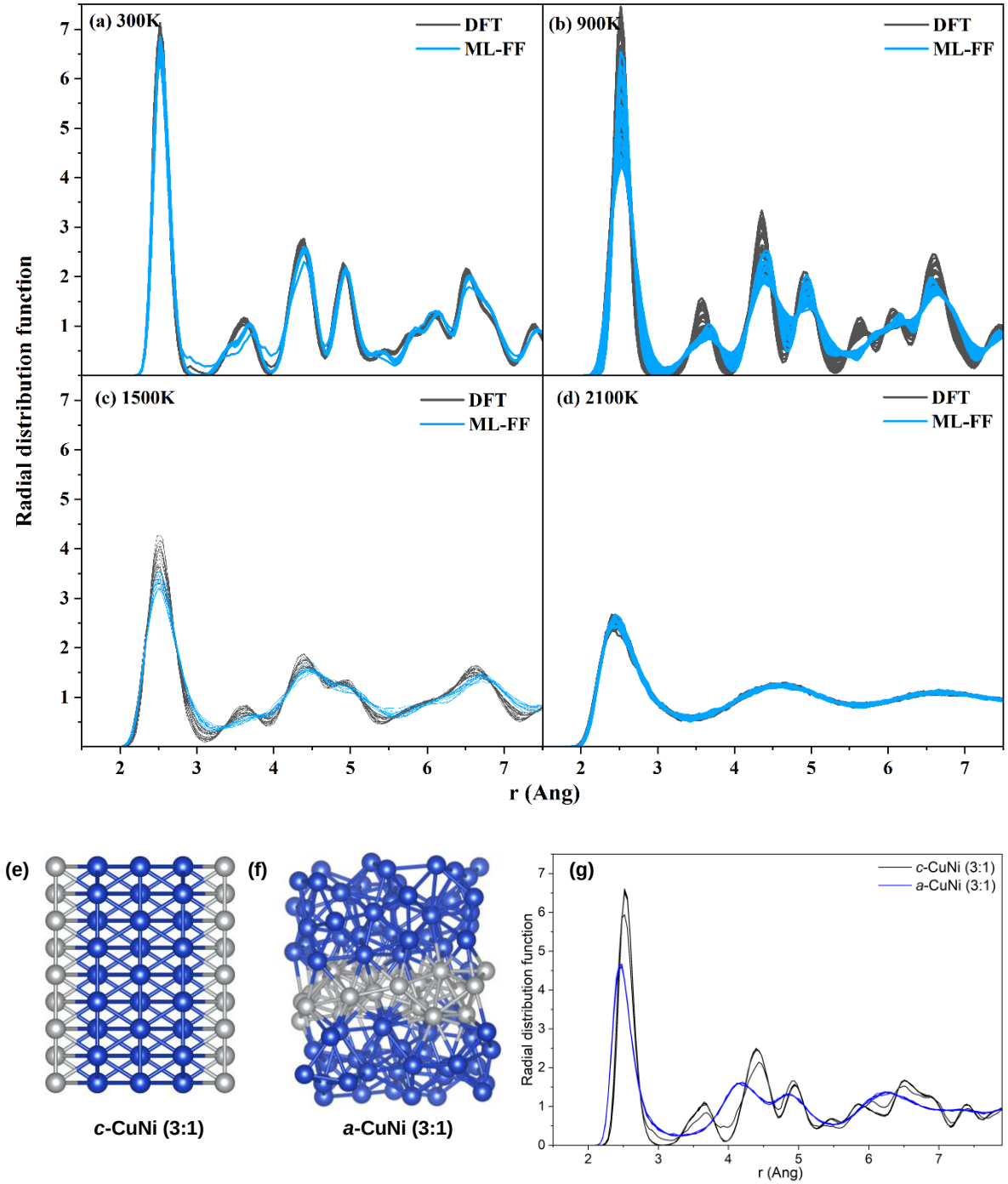

Figure S1: Comparison of the radial distribution functions (RDFs) of bulk CuNi computed using *ab initio* molecular dynamics (AIMD, black line) and machine-learned force field molecular dynamics (ML-FF MD, blue line) in the NPT ensemble at four different temperatures: (a) 300 K, (b) 900 K, (c) 1500 K, and (d) 2100 K.

Characterization of amorphous CuNi surfaces

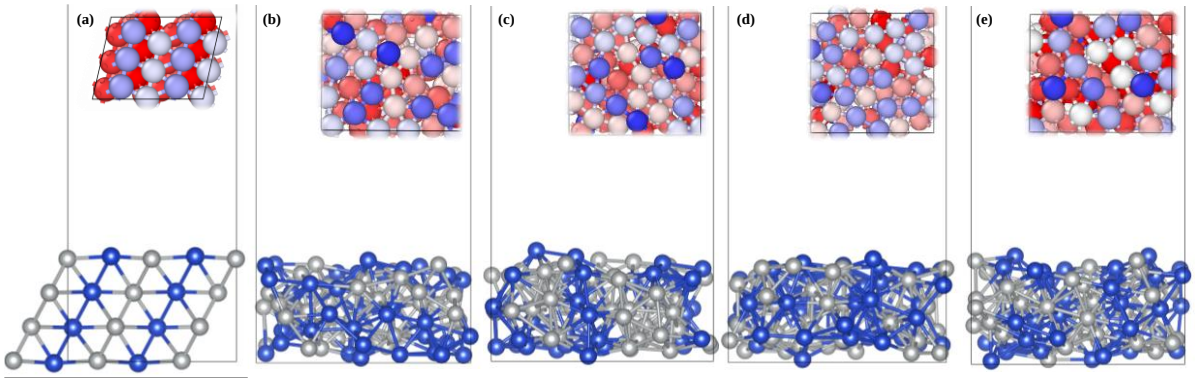

Figure S2. Surface structures of (a) crystalline CuNi(111) and amorphous CuNi surfaces: (b) CuNi(i), (c) CuNi(ii), (d) CuNi(iii), and (e) CuNi(iv). The images are color-coded to represent the coordination number (CN) of surface atoms, highlighting structural and coordination differences across the models.

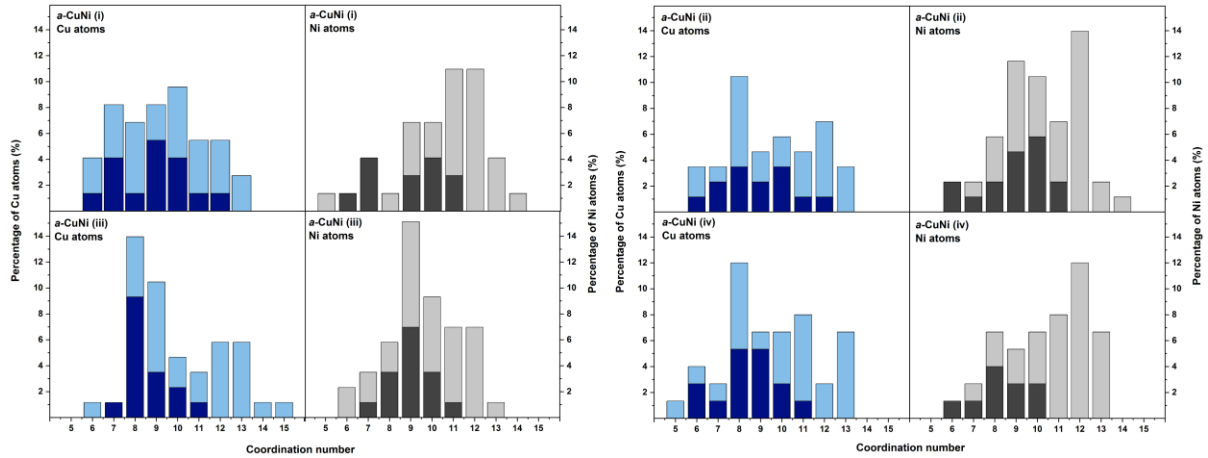

Figure S3: Coordination number (CN) analysis of Cu and Ni atoms of (a) CuNi(i), (b) CuNi(ii), (c) CuNi(iii), and (d) CuNi(iv) Grey bars: CN of all atoms in the surface model. Blue bars: CN of surface atoms only.

Table S1: Surface energy (γ,° in eV Å^{-2}), and *d*-band center ($\delta\varepsilon_d$, in eV) of crystalline and amorphous CuNi surfaces.

System	γ	$\delta\varepsilon_d$
***c*-CuNi (111)**	0.262	-1.530
***a*-CuNi (i)**	0.245	-1.597
***a*-CuNi (ii)**	0.247	-1.535
***a*-CuNi (iii)**	0.241	-1.581
***a*-CuNi (iv)**	0.250	-1.573

Optimized structures of CO_2 adsorbed on crystalline *c*-CuNi (111) and amorphous *a*-CuNi(i) surfaces

System	ΔE_{CO2}	*CO_2 optimized structures
***c*-CuNi (111)**		
Chemisorption	-1.88	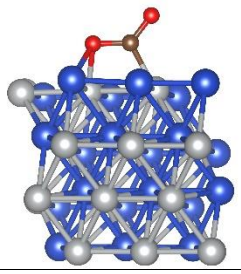
	-1.68	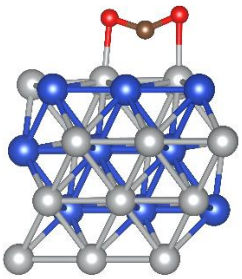
Physisorption	-1.73	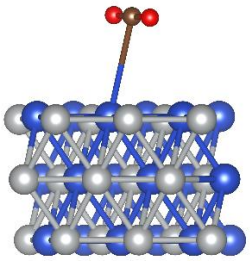
	-1.64	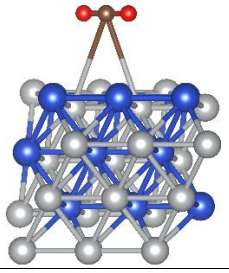
	-1.63	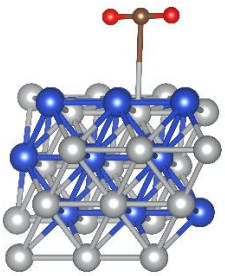
***a*-CuNi (i)**		

Chemisorption	-0.70	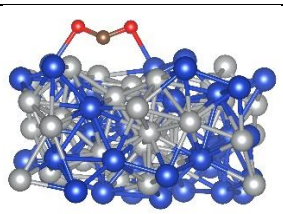
	-0.64	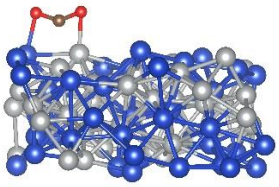
	-0.60	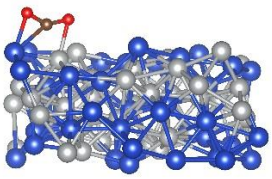
	-0.59	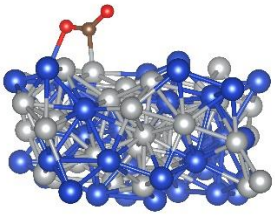
	-0.30	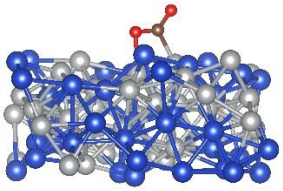
	-0.28	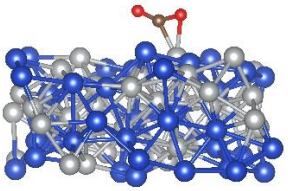
Physisorption	-0.81	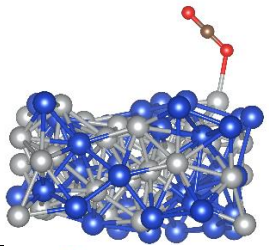
	-0.30	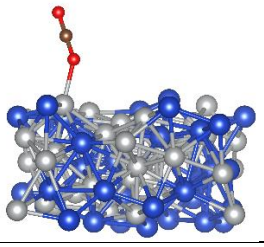

	-0.27	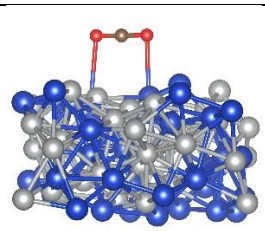
	-0.26	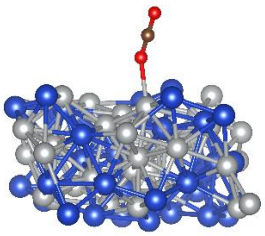
	-0.25	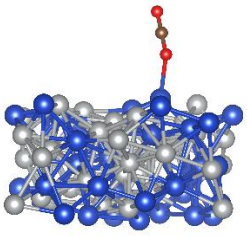

Figure S4: Optimised structures of adsorbed CO_2 on the crystalline *c*-CuNi(111) surface and *a*-CuNi(i) surface.

Table S2: Coordination number (CN) of the Cu and Ni active sites, adsorption energy (ΔE_{CO_2} , in eV), C–O bond length ($d_{C–O}$, in Å), O–C–O bond angle (θ_{OCO}, in degrees) of CO_2 adsorbed on amorphous CuNi surface labelled *a*-CuNi(ii).

System	CN		ΔE_{CO_2}	$d_{C–O}$	θ_{OCO}
	Cu	Ni			
***a*-CuNi (ii)**					
Chemisorption	-	6	-1.31	1.29, 1.21	149.0
	-	8,7	-1.87	1.25, 1.24	140.0
	-	7,6	-2.19	1.25, 1.24	139.0
Physisorption	7	-	-0.84	1.17, 1.18	180.0
	-	6	-0.94	1.18, 1.18	179.4
	-	6	-1.59	1.18, 1.17	179.4

Electrochemical CO_2 reduction to C_1 products (CO and HCOOH) on the crystalline *c*-CuNi(111) surface and amorphous *a*-CuNi(i) surface.

Gas-phase	OCHO*	COOH*	CO*
c-CuNi(111)	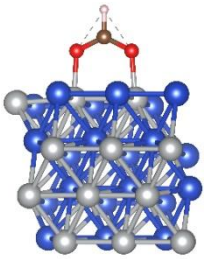	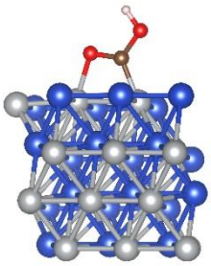	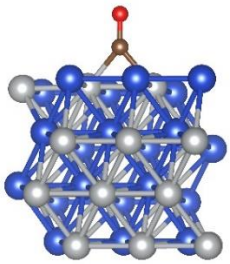
a-CuNi(i)-site a	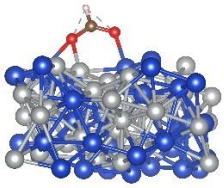	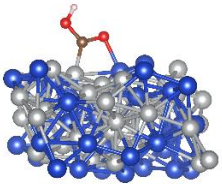	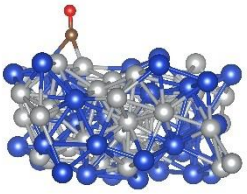
a-CuNi(i)-site b	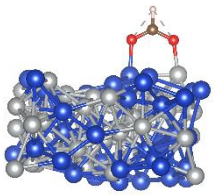	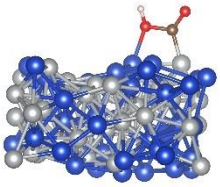	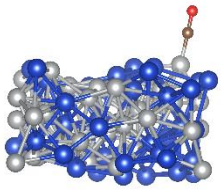
a-CuNi(i)-site c	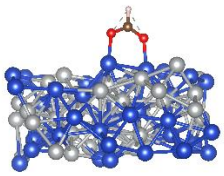	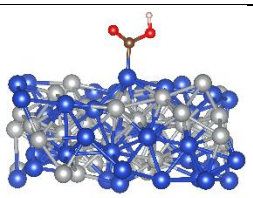	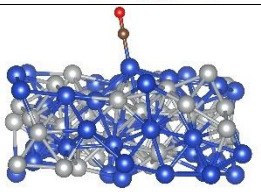

Figure S5: Optimised structures of the *OCHO, *COOH, and *CO intermediates on *c*-CuNi (111) and *a*-CuNi(i) surfaces.

Electrochemical CO_2 reduction to ethanol (C_2H_5OH) and ethylene (C_2H_4) on the crystalline *c*-CuNi (111) surface.

System	**c-CuNi (111)**		
Ethanol		**Ethylene**	
*CO + *CHO	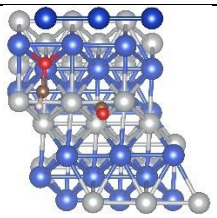	*CO + *CHO	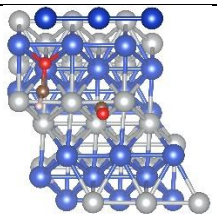
*COCHO	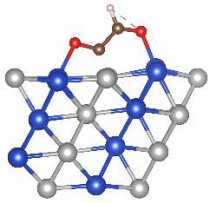	*COCHO	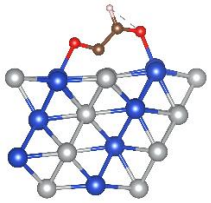
*OCHCHO	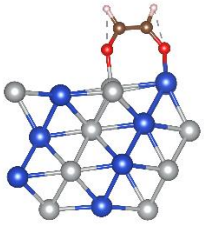	*OCH_2CO	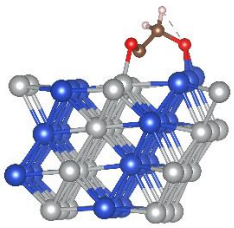
*OCH_2CHO	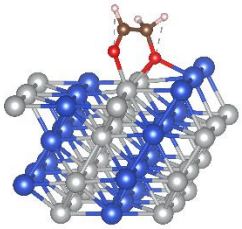	*OCH_2COH	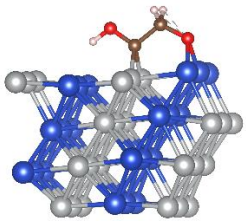
*$OHCH_2CHO$	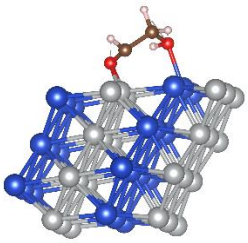	*OCH_2CHOH	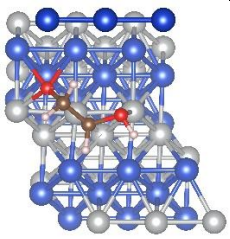
*CH_2CHO	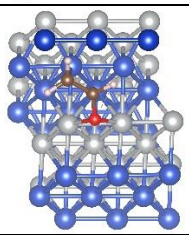	*OCH_2CH	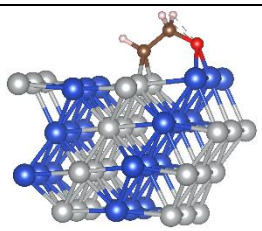
*CH_2CHOH	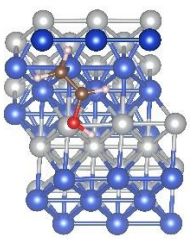	*OCH_2CH_2	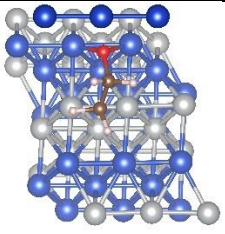

*CH_2CH_2OH	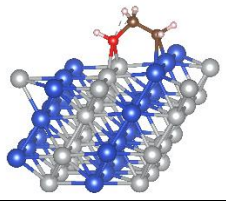	*O + CH_2CH_2	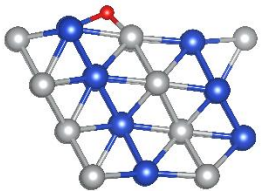

Figure S6: Optimised intermediates for the formation of ethanol (C_2H_5OH) and ethylene (C_2H_4) formation on *c*-CuNi (111) and *a*-CuNi(i).

Electronic properties of *COCHO adsorbed on crystalline *c*-CuNi (111) surface and amorphous *a*-CuNi(i) surfaces

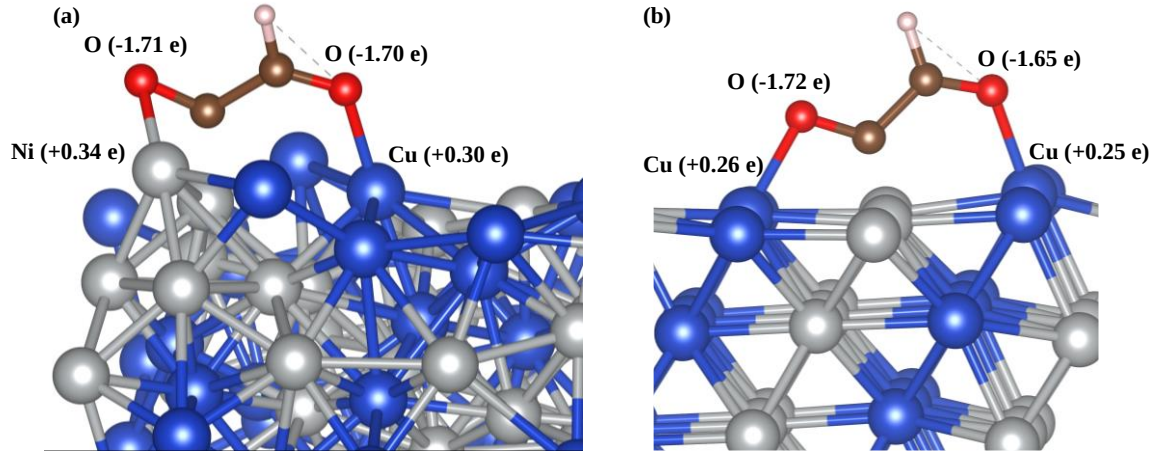

Figure S7: Bader charge analysis of Cu and Ni atoms in the surfaces, and O and C atoms in the adsorbed *COCHO intermediate on the (a) amorphous *a*-CuNi(i) and (b) crystalline *c*-CuNi (111) surfaces.

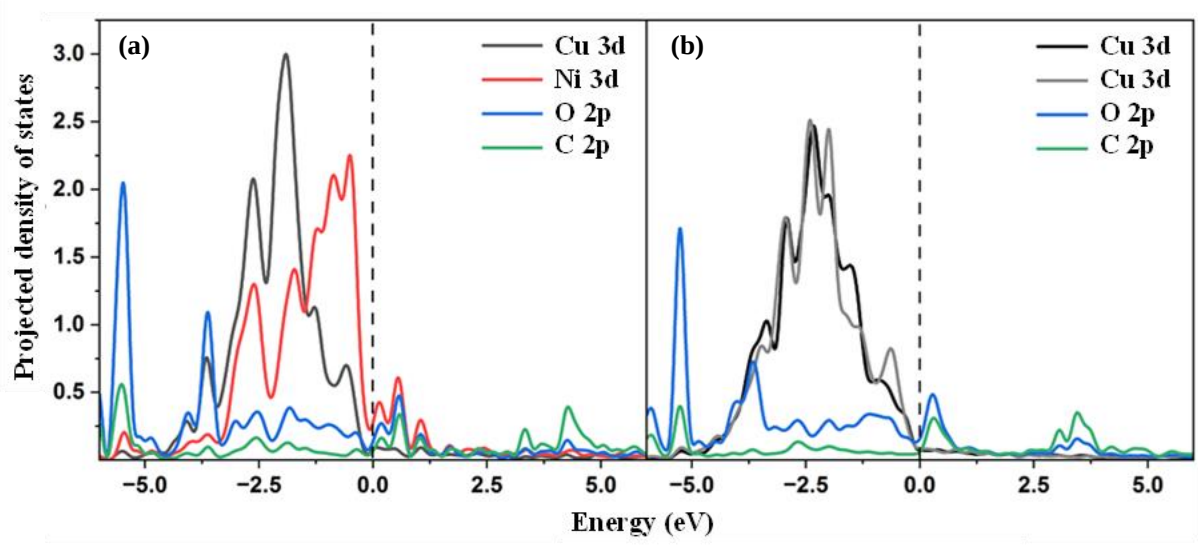

Figure S8: Projected density of states (PDOS) of 3d orbital contributions of Cu and Ni atoms, and the 2p orbital contributions of C and O atoms, for the *COCHO intermediate adsorbed on (a) *a*-CuNi(i) and (b) *c*-CuNi (111) surfaces.

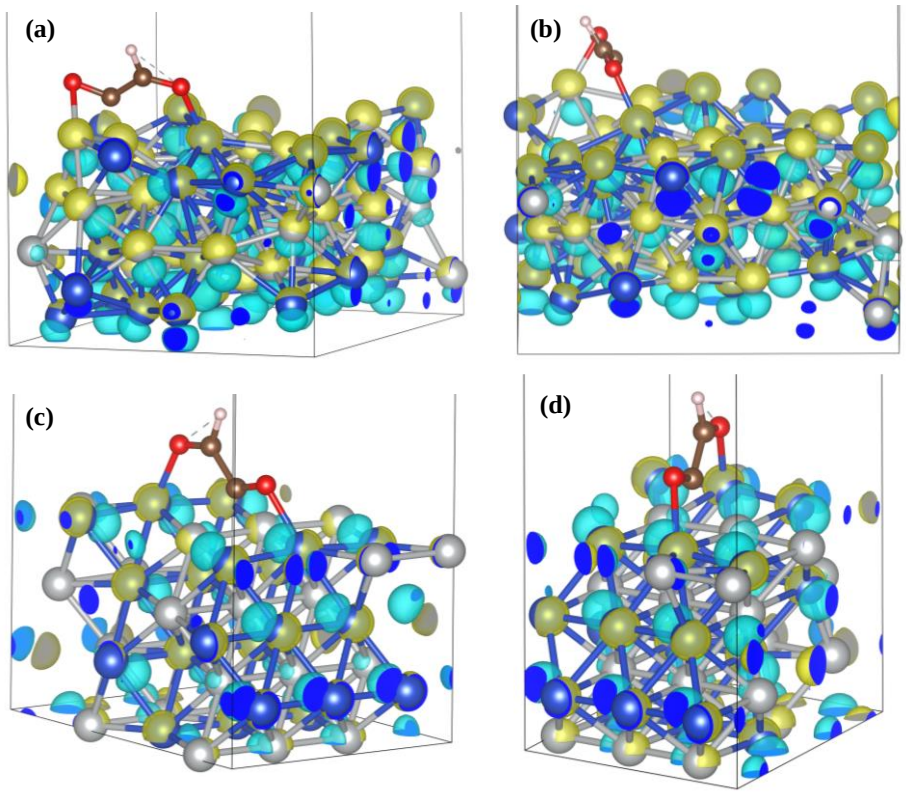

Figure S9: Charge density difference plots showing *COCHO on the (a–b) *a*-CuNi(i) and (b-c) *c*-CuNi (111) surfaces. Yellow and blue isosurfaces represent regions of electron accumulation and depletion, respectively

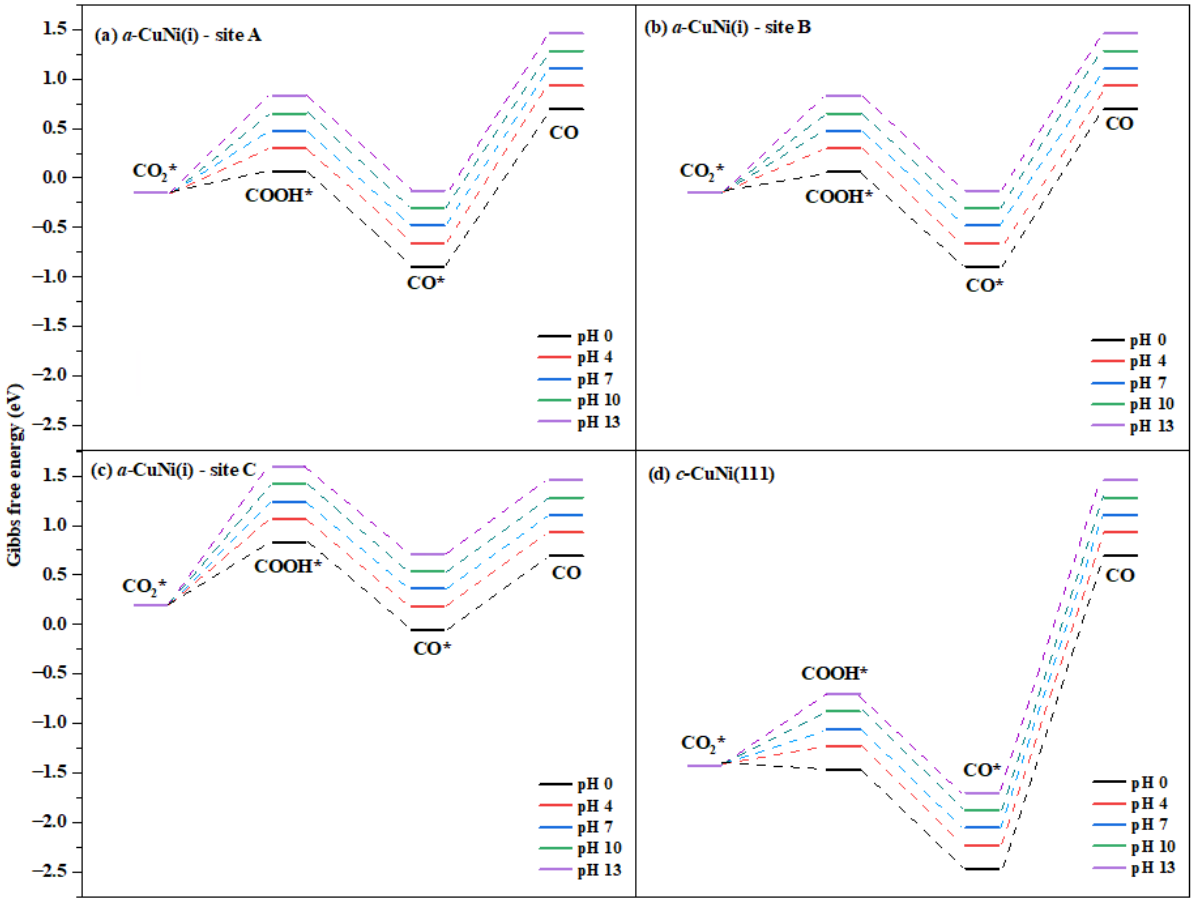

Figure S10: Gibbs free energy profiles for the CO_2 reduction reaction to CO at varying pH values (0, 4, 7, 10, and 13) on: (a) site A, (b) site B, and (c) site C of *a*-CuNi, and (d) *c*-CuNi(111).